Journal of Rock Mechanics and Geotechnical Engineering 8 (2016) 443–461

Contents lists available at ScienceDirect

Journal of Rock Mechanics and Geotechnical Engineering

journal homepage: www.rockgeotech.org

Full length article

Dynamic design method for deep hard rock tunnels and its application

Xia-Ting Feng*, Chuanqing Zhang, Shili Qiu, Hui Zhou, Quan Jiang, Shaojun Li

State Key Laboratory of Geomechanics and Geotechnical Engineering, Institute of Rock and Soil Mechanics, Chinese Academy of Sciences, Wuhan, 430071, China

ARTICLE INFO

Article history:
Received 19 November 2015
Received in revised form
23 January 2016
Accepted 24 January 2016
Available online 19 May 2016

Keywords:
Deep hard rock tunnels
Dynamic design method
Rockburst
In situ stress
Constitutive model

ABSTRACT

Numerous deep underground projects have been designed and constructed in China, which are beyond the current specifications in terms of scale and construction difficulty. The severe failure problems induced by high in situ stress, such as rockburst, spalling, damage of deep surrounding rocks, and time-dependent damage, were observed during construction of these projects. To address these problems, the dynamic design method for deep hard rock tunnels is proposed based on the disintegration process of surrounding rocks using associated dynamic control theories and technologies. Seven steps are basically employed: (i) determination of design objective, (ii) characteristics of site, rock mass and project, and identification of constraint conditions, (iii) selection or development of global design strategy, (iv) determination of modeling method and software, (v) preliminary design, (vi) comprehensive integrated method and dynamic feedback analysis, and (vii) final design. This dynamic method was applied to the construction of the headrace tunnels at Jinping II hydropower station. The key technical issues encountered during the construction of deep hard rock tunnels, such as in situ stress distribution along the tunnels, mechanical properties and constitutive model of deep hard rocks, determination of mechanical parameters of surrounding rocks, stability evaluation of surrounding rocks, and optimization design of rock support and lining, have been adequately addressed. The proposed method and its application can provide guidance for deep underground projects characterized with similar geological conditions.

1. Introduction

With the strategic planning of major projects, such as West-to-East Power Transmission, South-to-North Water Transfer, highway and high-speed railway networks, more than 20 large-scale water conservancy and hydropower projects have been built or planned in the areas with high mountains and deep gorges in western China. The total length of transportation tunnel projects exceeds 10,000 km. Some projects are characterized by great depth, complicated geological conditions, active tectonic movements, and high in situ stress, which are rarely reported in the world. In addition, exploitation of large-scale deep metal mineral resources has become a trend in China's mining industry. For example, a large number of nonferrous metal mines, such as Fankou lead-zinc mine and Dongguashan copper mine, have approached to deep mining. The exploration depth of metal mineral resources such as iron can reach 2000–4000 m. In Dataigou iron mine, Chentaigou iron mine, Sanshandao gold mine, and Jining iron mine, the mineral deposits at depth over 1800 m are reported. It can be expected that in the near future, the exploration of metal mineral resources in China will exceed 1000 m below the surface, making China one of the countries be characterized with greatest mining depth.

With the increase in mining depth and engineering scale of construction projects, deep engineering disasters (e.g. large-scale collapse and intensive rockburst) are observed frequently with wide range and severe damage. This poses great challenges to the design and optimization of deep hard rock tunnels and to the disaster prevention and control. The following issues concerning disaster prevention and control should be concentrated on:

(1) The formation and evolution of excavation damaged zone (EDZ) during construction;

* Corresponding author. Tel.: +86 27 87198913.
E-mail address: xtfeng@whrsm.ac.cn (X.-T. Feng).

Peer review under responsibility of Institute of Rock and Soil Mechanics, Chinese Academy of Sciences.

http://dx.doi.org/10.1016/j.jrmge.2016.01.004

(2) The mechanism of rockburst, stress-induced collapse and other types of disasters;
(3) The theory to predict the formation and evolution of the EDZ and the induced disasters;
(4) The dynamic regulation based on the formation of EDZ and development of disasters.

To address above-mentioned issues, a systematic investigation is mandatory to understand the disintegration process of surrounding rocks and to determine the corresponding dynamic control theories and technologies (Feng et al., 2013a).

In this context, the dynamic design method is proposed in conjunction with the characteristics of deep hard rock tunnels (Fig. 1). Then, the engineering practices of the proposed method for the deep headrace tunnels at Jinping II hydropower station are discussed, which can facilitate planning, design and analysis of similar deep engineering projects.

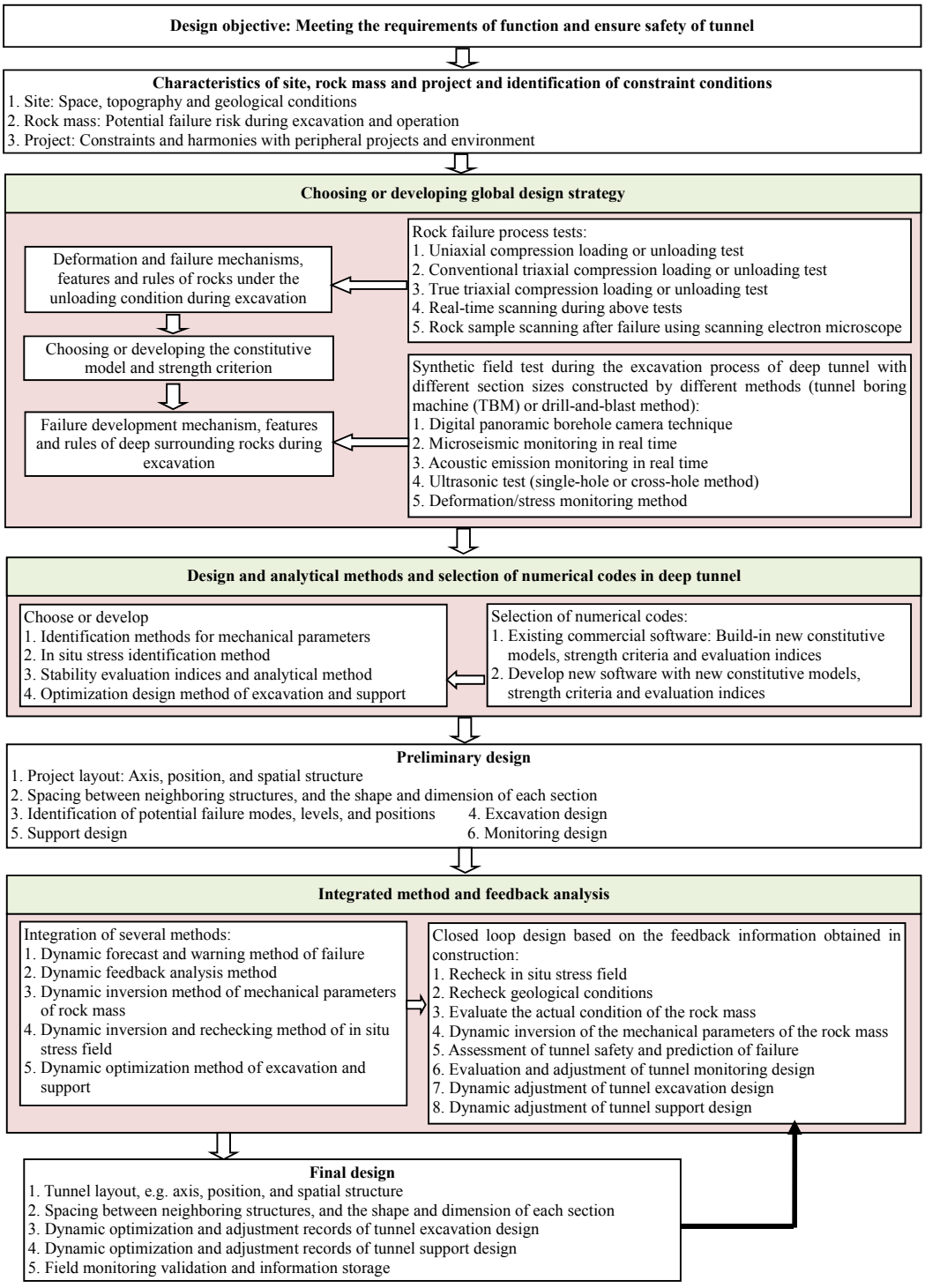

Fig. 1. Flowchart of dynamic design method for deep hard rock tunnels (Feng et al., 2013a).

(a) Rockburst. (b) Rib spalling.

(c) Slabbing. (d) Cracking.

Fig. 2. Typical rock failures under high stress conditions.

2. Design principles of deep hard rock tunnels

2.1. Design objective

The design objective of the deep hard rock tunnels is to determine the tunnel dimensions, cross-section shape, and spacing which can meet the functional requirements and the stability standards during the lifetime of a tunnel. In addition, it aims at the determination of the excavation and support methods, and the risks based on the geological conditions, time limit, and tunnel function. The requirements of function and safety during the lifetime of a tunnel vary from different kinds of tunnels:

(1) Large headrace tunnels in large hydropower stations should meet the safety and stability requirements throughout the specified service period (e.g. 100 years) under coupling of internal and external water pressures.
(2) Transportation tunnels should meet the safety and stability requirements throughout their service period.
(3) Military tunnels should meet the safety and stability requirements of long-term operation and external attack.
(4) Mine transportation shafts, tunnels, ramps and entryways should meet the safety and stability requirements throughout the mining and production periods.
(5) Tunnels in areas with high seismic intensity should consider the specific safety and stability requirements imposed by earthquakes.
(6) For tunnels and chambers of radioactive waste repositories, the EDZ size in surrounding rocks should be controlled to the minimum during construction, and the stability of surrounding rocks under the coupling effects of temperature, water flow, stress and chemical solutions should be ensured.

2.2. Site characteristics and identification of geological constraints

The site characteristics of tunnels include geological conditions, in situ stresses, hydrogeological conditions, seismic intensity, rock mass features, topography, tunnel positions and axis, and so on. The magnitudes and directions of in situ stresses will affect the direction of tunnel axis, dimensions of tunnel cross-sections, tunnel groups,

Fig. 3. Water inrush in a deep hard rock tunnel.

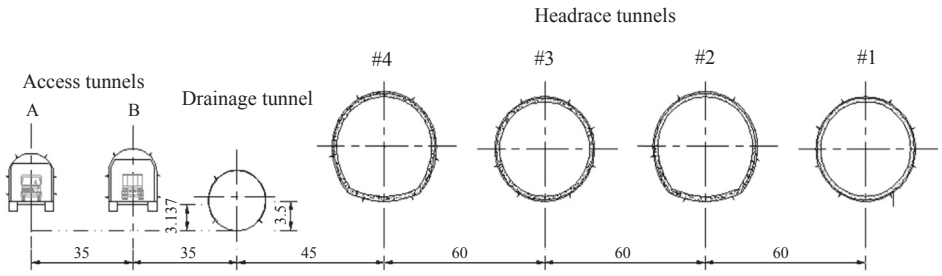

Fig. 4. Layout of tunnels in Jingping II hydropower station (unit: m).

and tunnel spacing. The factors affecting the tunnel spacing include rock mass properties and mutual interference induced by excavation.

The tunnel axis should be parallel to the maximum principal stress or intersect at a small angle. For example, deep headrace tunnels need to be arranged based on the inlet topography and water sources conditions, the outlet powerhouse location, generating units layout, and water power requirements. The arrangement of the tunnels should be coordinated with neighboring engineering projects and the environments.

The rock mass properties and identification of their constraints include the mechanical properties of rock mass, i.e. strength and deformation properties and their variation upon unloading, and the following problems during excavation:

(1) Hard rock failures under high in situ stress conditions, such as rockburst, hard rock cracking, rib spalling, slabbing, and stress-induced collapse (Fig. 2);
(2) Development of faults, joint fissures, columnar joints, and dislocation bands (e.g. massive collapse);
(3) Groundwater development and high water pressure problems, such as water and mud outburst (Fig. 3).

3. Design strategy of deep hard rock tunnels

Upon tunnel design, different design schemes should be proposed and evaluated under site-specific conditions, thus performing the model-based prediction is necessary. The model used should be based on the tunnel type and potential risks encountered during construction. A good global design strategy includes reasonable tunnel axis arrangement, spacing, and global optimization of excavation and support, thereby reducing the depth and extent of surrounding rock loosening, stress-induced collapses, risk and damage caused by rockburst, and maintaining the long-term bearing capacity of surrounding rocks. This can be implemented using the following four methods.

(1) Numerical methods

(i) Mechanical models and strength criteria should basically reflect the mechanism of hard rock unloading failure under high in situ stress conditions;
(ii) Evaluation indices: (a) Failure approach index (FAI) evaluating the damage degree and its evolution at different parts of deep rocks after excavation, and (b) local energy release rate (LERR) describing the magnitudes of energy release during excavation at different parts of deep rocks (Feng et al., 2013b);
(iii) Basic numerical methods (e.g. finite element method and continuous–discontinuous cellular automaton method) used in the above-mentioned models and the associated indices can represent the unloading effect, formation and evolution of the EDZ. The effects of different types of supports, and the position and depth of rockburst, stress-induced collapse, and loosening of surrounding rocks can be estimated.

(2) Rock mass classification methods

(i) Rock mass classification methods, such as basic quality index (BQ), rock mass rating (RMR), Q-system, Q_{TBM}-system, and China's rock classification standard;
(ii) The rockburst classification method and related surrounding rock classification method should be improved upon the excavation and support strategies for different grades of rockbursts.

(3) Artificial intelligence methods

(i) Expert systems for rockburst risk estimation, such as the expert systems used in South Africa's deep gold mine VCR mining field, coal mines and tunnels;

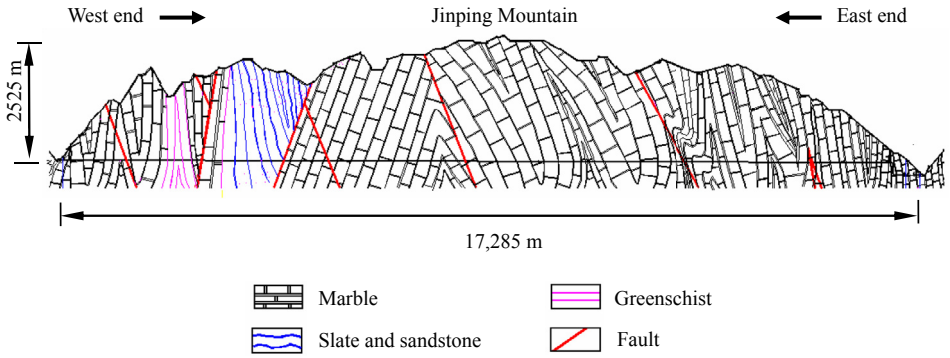

Fig. 5. Geological profile along headrace tunnels in Jinping II hydropower station.

Fig. 6. Extremely intensive rockburst in auxiliary tunnel B in Jinping II hydropower station.

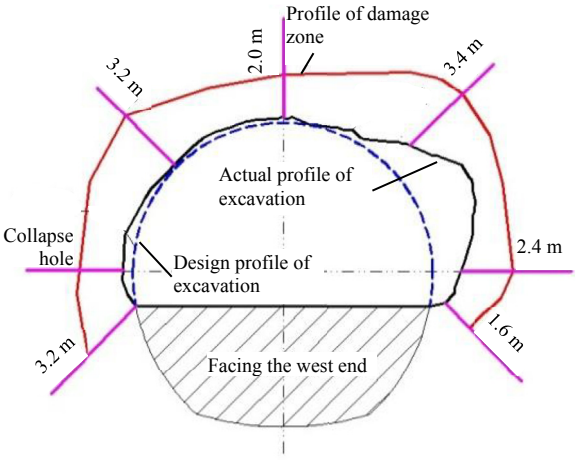

Fig. 8. EDZ at stake k11 + 025 in headrace tunnel #2 in Jinping II hydropower station.

(ii) Neural network models for rockburst risk estimation, such as the neural networks used in South Africa's deep gold mine VCR mining field, coal mines and tunnels, and the engineering practice-based neural network models for rockburst grade and pit depth estimation;
(iii) Neural network model for rockburst grade and pit depth warning based on the evolution of micro-seismic information.

(4) Comprehensive integration methods

(i) Intelligent inversion method to determine the mechanical parameters of deep rocks integrating with sensitivity analysis, numerical calculation, neural network, genetic algorithm (GA) (or particle swarm algorithm), and correlation analysis;
(ii) Dynamic feedback analysis of hard rock tunnel stability based on dynamic update of geological information, rock mass actual condition, and local failure mode;
(iii) Excavation and support dynamic optimization method based on early-warning, dynamic update of field geological and rock mass conditions, and local failure mode.

Fig. 7. "11.28" extremely intense rockburst in the drainage tunnel in Jinping II hydropower station.

For the above-mentioned methods, a series of laboratory rock mechanics tests, especially the loading and unloading tests that can reflect the unloading process of deep rocks during excavation, should be carried out to represent the mechanism, characteristics, and rules of deformation and failure of rock samples under high-stress unloading conditions. Based on these findings, suitable mechanical model and strength criterion are selected or established, and compared with the test results.

4. Analysis and design method of deep hard rock tunnels

To address the potential engineering problems in deep hard rock tunnels, the following methods and software need to be considered:

(1) Identification method of rock mass mechanical parameters, e.g. the intelligent inversion method based on displacement and EDZ information, which considers the evolution of rock mass mechanical parameters and the damage degree;
(2) In situ stress identification, e.g. the three-dimensional (3D) nonlinear inversion method for in situ stress field estimation considering the tectonic movement history of geological structures;
(3) Safety and stability evaluation index and method, e.g. FAI and LERR;
(4) Excavation and support optimization design method, e.g. fracture-inhibition method, and particle swarm-support vector machine (neural network) global optimization method using LERR and elastic energy release as key variables;
(5) Large-scale commercial software FLAC and ABAQUS, which integrates new mechanical model, strength criterion, and evaluation index such as FAI and LERR;
(6) New software development, e.g. continuous–discontinuous cellular automaton method that considers non-compatible deformation failure process, and integrates with new mechanical model, criterion and index.

5. Preliminary design of deep hard rock tunnels

Based on the global optimization and design strategy as mentioned in Sections 2–4, the preliminary design of deep hard rock tunnels includes the following aspects:

(1) Engineering project layout, e.g. tunnel axis, position and spatial structure;
(2) Spacing between engineering structures, and the cross-section shape and dimensions;
(3) Identification of possible failure mode (e.g. rockburst, stress-induced collapse, and fault slip), failure degree (FD), and failure position;
(4) Excavation design, e.g. excavation method, cross-section dimensions, daily footage, position, and advanced distance of pilot tunnel;
(5) Support design, e.g. selection of support type and determination of support parameters;
(6) Monitoring design, e.g. surrounding rock stress, deformation, acoustic wave, micro-seismicity, acoustic emission, and support system loading condition.

6. Integrated model and feedback analysis of deep hard rock tunnels

Based on the geological conditions, major engineering problems, rock mass deformation and failure mechanism, failure modes, and requirement of design objective, the integrated method basically includes the following aspects:

(1) Tunnel failure dynamic early-warning method, e.g. the rockburst intensity and early-warning probability method based on the micro-seismicity information, and the neural network early-warning method of rockburst intensity and pit depth based on the analogy of actual micro-seismicity information;
(2) Tunnel dynamic feedback analysis based on dynamic update of geological information and rock mass actual information;

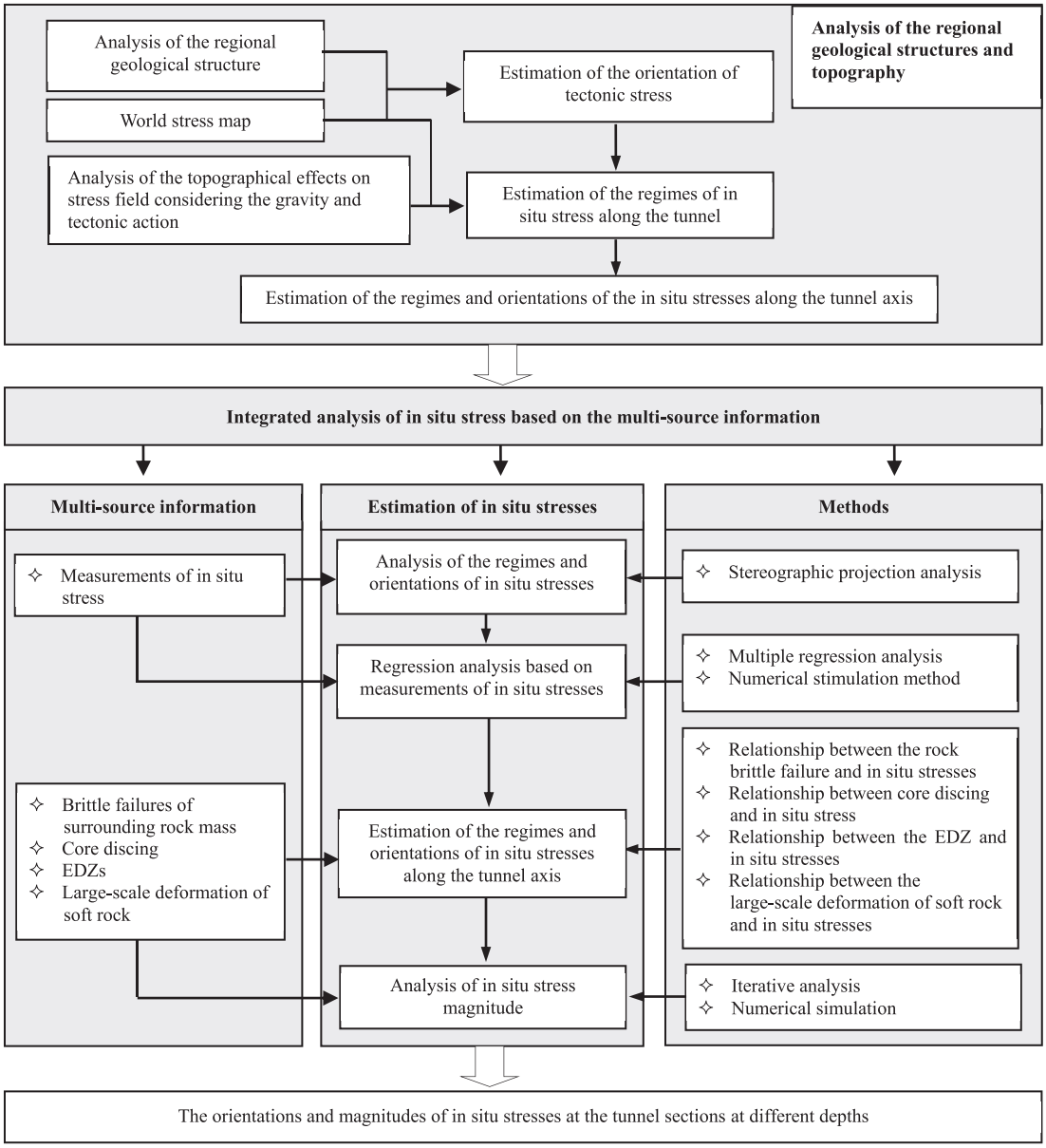

Fig. 9. Workflow of estimation method of in situ stress along deep tunnel axis (Zhang et al., 2011).

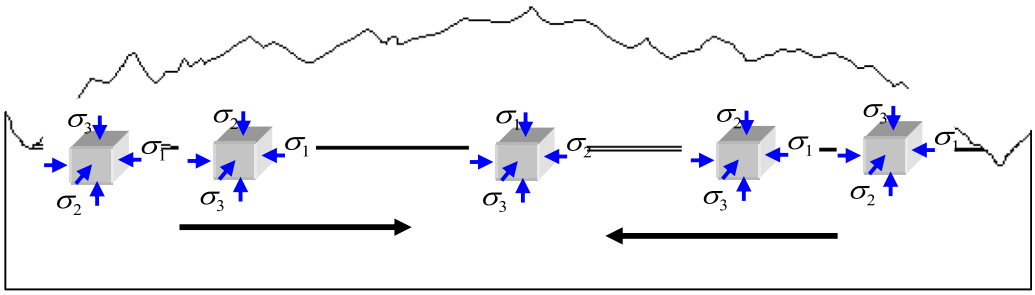

Fig. 10. Prediction of macro-distribution of in situ stress along headrace tunnels in Jinping II hydropower station. σ_1, σ_2 and σ_3 denote the maximum, intermediate and minimum principal stresses, respectively.

(3) Dynamic inversion method for determination of rock mechanical parameters, e.g. the inversion method based on field surrounding rock status after excavation;
(4) Dynamic inversion rechecking method for determination of in situ stress field, e.g. the rechecking method based on on-site surrounding rock deformations, and stress-induced failure position;
(5) Dynamic optimization method for excavation and support designs, e.g. the dynamic optimization method based on new indices (e.g. FAI and LERR), dynamic update of geological information, field rock mass status information, local failure mode, and micro-seismicity early-warning prediction.

The dynamic design is implemented based on the following feedback information during the construction:

(1) Rechecking of in situ stress field;
(2) Rechecking of geological conditions;
(3) Evaluation of actual condition of rocks;
(4) Dynamic inversion of mechanical parameters of rocks;
(5) Assessment of tunnel safety and prediction of failure;
(6) Evaluation and adjustment of tunnel monitoring design;
(7) Dynamic adjustment of tunnel excavation design;
(8) Dynamic adjustment of tunnel support design.

7. Final design of deep hard rock tunnels

The final design of deep hard rock tunnels includes the following aspects:

(1) Tunnel arrangement, e.g. axis, position, and spatial structure;
(2) Spacing between engineering structures and the shape and dimensions of each section;
(3) Dynamic optimization and adjustment records of tunnel excavation design;
(4) Dynamic optimization and adjustment records of tunnel support design;
(5) On-site monitoring validation and information storage.

8. Application of dynamic design method to deep hard rock tunnels

8.1. Project description

The Jinping II hydropower station is located on the Yalong River in China. It has the highest water head and the largest installed capacity in China to date. The hydropower station mainly consists of sluice, headrace system, and underground powerhouse, which is a low-sluice, long-tunnel, and large-capacity headrace-type hydropower station. There are four headrace tunnels with an average tunnel distance of 16.67 km. The excavated tunnel diameter is 13 m, and the tunnel diameter with lining is 11.8 m, as shown in Fig. 4. The general overburden depth is 1500–2000 m, with the maximum depth of 2525 m, as shown in Fig. 5. This hydropower station is characterized by large-scale and ultra-depth (Wu et al., 2010).

More than 270 rockburst events were reported during the excavation of the auxiliary tunnels A and B, as shown in Fig. 6. Fig. 7 shows an extremely strong rockburst of a drainage tunnel during construction on 28 November 2009, where a depth of around 8 m from the crown burst was observed and rockburst destroyed the TBM major girder. These high-stress induced problems pose significant challenges to construction of the headrace tunnels.

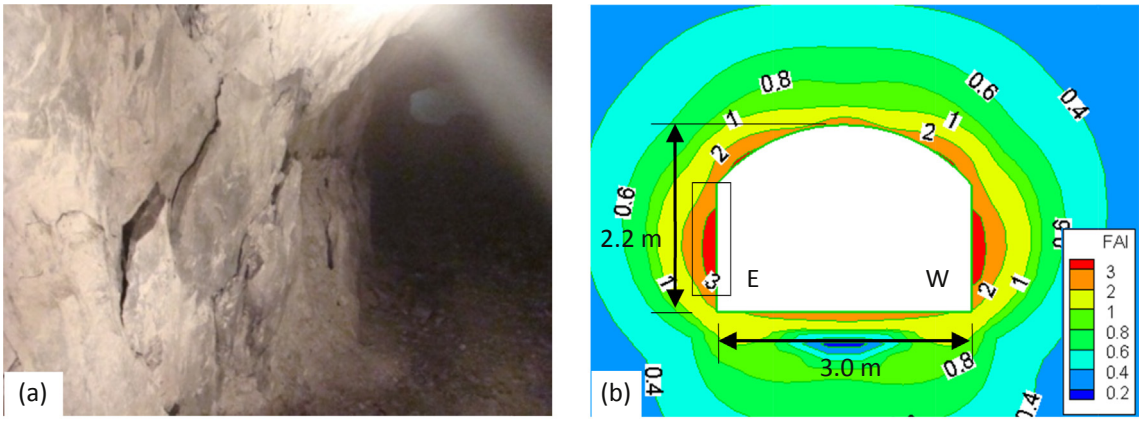

Fig. 11. (a) Brittle failures on east sidewall of test tunnel #2 and (b) distribution of FAI calculated at corresponding tunnel cross-section.

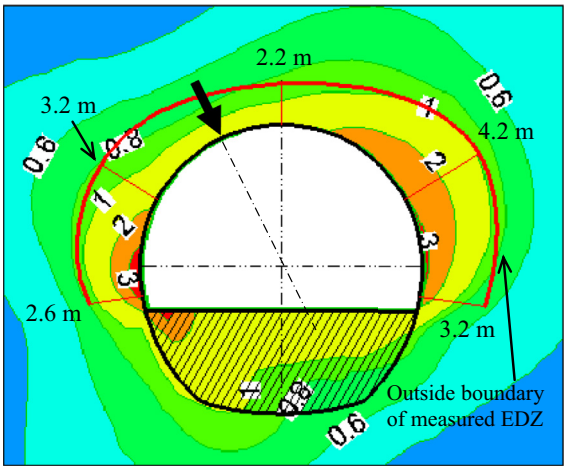

Fig. 12. Calculated and measured EDZs at section k9 + 810 in headrace tunnel #4. Large-font numbers are the FAI values.

Unlike dynamic failures such as rockburst, the majority of stability problems in the surrounding rocks during construction are static brittle failures (e.g. spalling and peeling) and deep fractures of surrounding rocks. Fig. 8 shows the depth of EDZ of surrounding rocks measured with acoustic wave test after rockburst. One can see that the depth of EDZ in the surrounding rocks of the whole section reached 3 m after rockburst, which, without timely support, will cause collapse and thereby delay the tunnel construction, and ultimately the normal operation.

The headrace tunnel is subjected to high in situ stress due to large overburden depth. The failure pattern of surrounding rocks is significantly different from that of shallow projects, which is mainly dominated by rockburst and static brittle failure. The problems associated with this type of tunnel are such complicated that current specifications are not suitable for combating those problems. In this circumstance, using dynamic design method for excavation and support may be helpful for solving these failure control problems.

8.2. Determination of in situ stress in field

The region of this project is significantly influenced by the tectonic movements that are frequently observed in western China, where the tectonic stress is very high, and the geological structures are well developed. The faults and folds have major influence on the in situ stress field along the tunnels, as observed by deep valleys and undulation of terrain. These factors make the in situ stress conditions along the tunnel axis very complicated. Meanwhile, due to the great depth and high in situ stress, the monitoring points are only set in tunnels with depth less than 1900 m. In deeper tunnels, because of drilling core damage, the stress relief method cannot be used, and the hydraulic fracturing technique cannot easily fracture the rock either. The acquisition of a detailed understanding of the in situ stress along the tunnel axis is a complex but fundamental problem.

A method of estimating in situ stress based on the analyses of macro-geological structure, topography and excavation response of local tunnel sections was proposed by Zhang et al. (2011). The workflow is shown in Fig. 9. Specifically, macro-field stress features are first analyzed based on the structural geology and topographic and terrain information. According to the characteristics of strong tectonic movements in the project site, the structural geology theory, combining with the geological conditions, is used to analyze the causes of regional tectonic movement, and to identify the direction of tectonic stress field. Meanwhile, the world stress mapping is introduced for comparison and verification. The influence of topographic characteristics on in situ stress distribution is investigated, and the overall in situ stress distribution along the tunnels can be obtained, as shown in Fig. 10.

Then, various technological means are employed to perform the integrated analysis of in situ stress at local tunnel sections based on multi-source information. According to the overall in situ stress distribution obtained, the in situ stresses of local tunnel sections are analyzed combining with multi-source information revealed during tunnel excavation (e.g. in situ stress testing information, position and FD of on-site surrounding rocks (Fig. 11), outline features of low acoustic wave zone (Fig. 12), drilling rock core discing, and soft rock squeezing deformation), and multiple technological means (e.g. multiple regression method, numerical simulation, stereographic projection, and iteration analysis).

Finally, the global and local analysis results are continuously verified according to updated information during excavation, thereby the in situ stresses of each section along the whole tunnel can be obtained.

8.3. Deformation and failure mechanism and mechanical model of hard rock under high stress and strong unloading

Deep rocks are subjected to high compressive stress environments before excavation. During excavation, the in situ stress is released in one direction, while increases in the other two directions. This may induce rockburst, static brittle failure (e.g. spalling and peeling), and collapse (sliding along cracking surface and structural surface). The stress variation during deep rock mass excavation indicates the necessity of performing loading and unloading tests to study the mechanical responses of rocks. The loading and unloading stress paths and unloading rate are the key factors that influence the mechanical properties of rocks during unloading process. However, currently there are few studies focusing on these factors; thus the test results are not able to be compared with other results. It is therefore necessary to establish reasonable triaxial loading and unloading test methods in axial and lateral directions to understand the effect of each factor on the loading and unloading processes. In this section, rock loading and unloading test methods and results are introduced, as shown in Fig. 13, and then the deep hard rock mechanical model and strength criterion are established based on the deformation and failure mechanism, mechanical properties, and mechanical evolution rules of rocks.

8.3.1. Loading and unloading test methods for hard rocks under high stress conditions

(1) Triaxial cyclic loading and unloading test method for hard rocks in axial direction

The aim of the triaxial cyclic loading and unloading test for hard rocks is to determine the mechanical parameters (strength parameters, deformation parameters, and dilatancy parameters) with the irreversible deformation or damage. The unloading process of axial load aims to determine the increments of irreversible deformation or damage for each cycle period.

During the test, the axial loading is controlled at a rate of 0.06 mm/min by axial displacement measured with the linear variable differential transformer (LVDT), and the unloading is controlled by axial force. For marbles T_{2y}^{4} and T_{2y}^{6}, the unloading rate is 30 kN/min (Zhang et al., 2010), and for marble T_{2b}, the unloading rate is 26 MPa/min. During the uniaxial unloading, the axial stress is unloaded to 98% of the initial axial stress, which is about 5 MPa. During unloading, the axial stress is unloaded approximately to the confining pressure level. When the unloading occurs at the peak or post-peak stage, the confining pressure is first

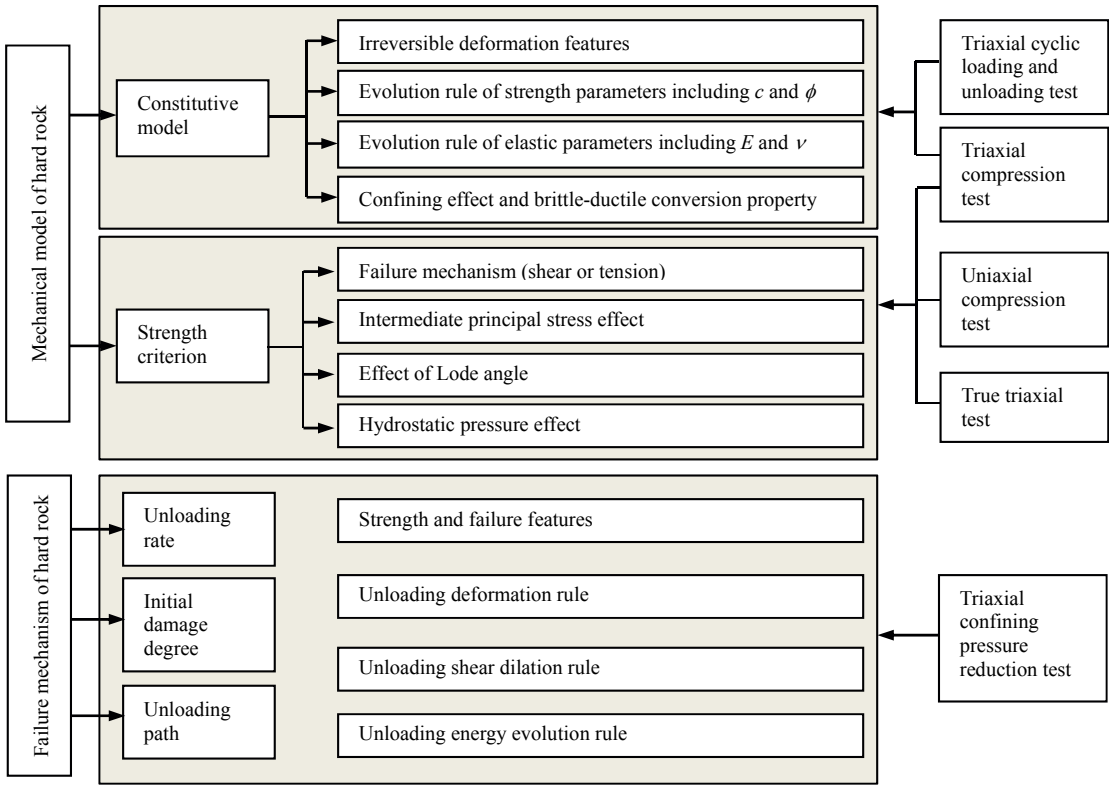

Fig. 13. Loading and unloading test contents and methods of hard rock under high in situ stress. c and ϕ are the cohesion and internal friction angle of rock, respectively; E is the Young's modulus; and ν is the Poisson's ratio.

increased by 1 MPa before unloading, and then removed during unloading. The test results on Jinping marble are shown in Fig. 14.

(2) Triaxial confining pressure unloading test method for hard rocks

The objective of the triaxial confining pressure unloading test for hard rocks is to represent the confining pressure unloading processes after the equilibrium of original 3D stress state is broken. This can facilitate the development of a strategy which is used to control the various factors affecting the mechanical properties of hard rocks during unloading, including unloading rate, initial damage degree, and stress path. It might also help to determine the evolution rules of mechanical parameters of hard rocks during unloading, e.g. strength parameters, deformation parameters, and dilatancy parameters, with irreversible deformation or damage.

The procedure for testing the unloading rate during triaxial confining pressure unloading test is described as follows:

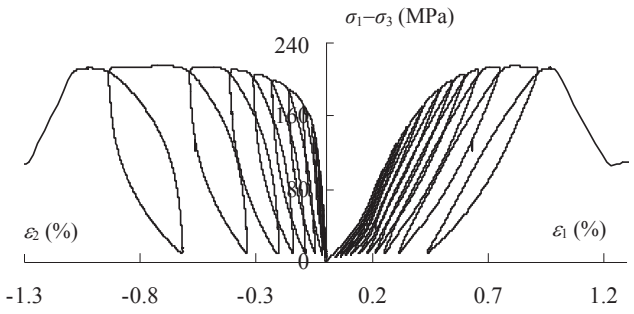

Fig. 14. Typical post-peak stress-strain curves of Jinping marble obtained through cyclic loading and unloading tests. ε_1 and ε_2 are the axial and lateral strains, respectively.

(1) The initial confining pressure σ_3 is preset equal to the hydrostatic pressure.
(2) The axial pressure σ_1 is increased to the designed value, which is 80% of the peak strength (equal to the stress level where volumetric strain reverses from negative to positive) based on the conventional triaxial compression test, and then it is kept constant.
(3) The confining pressure is unloaded at different rates until rock failure. Five unloading rates are 0.01 MPa/s, 0.1 MPa/s, 0.3 MPa/s, 0.5 MPa/s, and 1 MPa/s. The preset values of initial confining pressure are 10 MPa, 20 MPa, 40 MPa, and 60 MPa.

The ultimate strengths at different unloading rates of confining pressure are shown in Fig. 15. Within the range of 0.01–1 MPa/s, both high and low unloading rates increase the short-term strength of marble, suggesting that the short-term strength of deep marble is closely related to the unloading rate. Fig. 16 displays the evolution of dilatancy angle at an unloading rate of 0.1 MPa/s. Under high confining pressure conditions, as unloading rate increases, the dilatancy first increases and then decreases, indicating that the deformation characteristics of deep marble are related to the unloading rate.

In the unloading tests with different initial damage degrees, the confining pressure levels are 10 MPa, 20 MPa, 40 MPa, and 60 MPa, respectively. At each confining pressure level, three initial axial pressure levels are 60%–97% of the peak strength used in the triaxial compression test. The unloading rate is 0.3 MPa/s, and the confining pressure unloading path with constant axial pressure is selected. The procedures are described as follows:

(1) The initial confining pressure σ_3^0 is preset equal to the hydrostatic pressure.

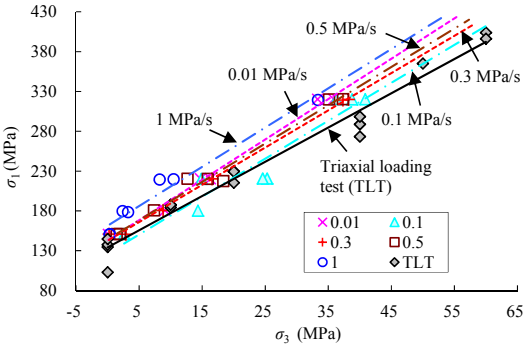

Fig. 15. Strength values of marble T^5_{2y} under different unloading rates of confining pressure (Qiu et al., 2010).

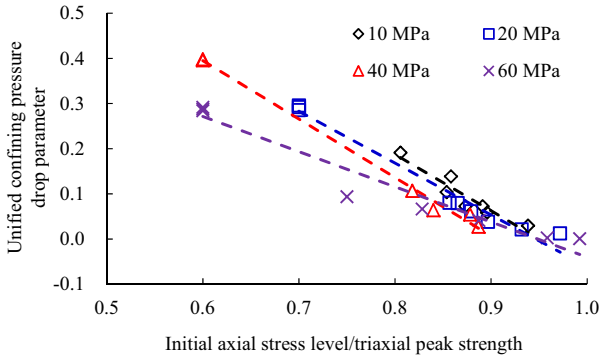

Fig. 17. Rock strength features of Jinping marble under different degrees of initial damage (Qiu et al., 2012).

(2) The axial pressure σ_1 is increased to the designed value, which is 60%–97% of the peak strength based on the triaxial compression test to meet the requirements of different degrees of initial damage, and then it is kept constant.
(3) The confining pressure is unloaded at 0.3 MPa/s until rock fails.

Fig. 17 shows the rock strength characteristics with different degrees of initial damage. By increasing initial confining pressure, the decrease rate of unified confining pressure drop parameter continuously reduces, suggesting that the unloading at high confining pressure, even with small amount of initial damage, can force the rock towards failure. The unified confining pressure drop parameter is the ratio of the reduced value at failure to the initial value of the confining pressure. Fig. 18 shows that the increase in initial damage can mobilize the rock dilatancy effect during unloading. However, the ratio of irreversible deformation to the total deformation still increases, indicating a more stable dilatancy process.

The unloading path should be determined based on the test objective. When studying the influences of unloading rate and initial damage on rock mechanical properties, the confining pressure unloading path with constant axial pressure is suggested. When studying the influence of unloading path on rock mechanical properties, the confining pressure unloading path with increasing or constant axial pressure is suggested. These two paths can approximately reflect the stress paths of deep rocks. Fig. 19 shows a comparison of ultimate bearing strengths of rocks under two unloading paths, suggesting that the unloading path will, to a certain extent, influence the rock deformation characteristics, but has a minor effect on the rock strength.

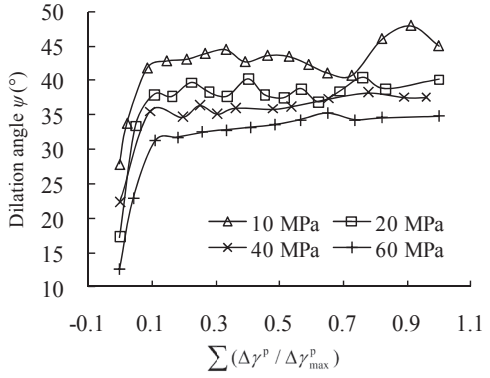

Fig. 16. Dilation angle evolution of marble T^5_{2y} in whole unloading process obtained by confining pressure unloading test at unloading rate of 0.1 MPa/s (Qiu et al., 2010). $\Delta\gamma^p$ is the plastic shear strain increment, and $\Delta\gamma^p_{max}$ is the maximum plastic shear strain increment.

8.3.2. Strength criterion of deep hard rocks

Generally, the strength criterion of hard rocks is depicted as a smooth, convex surface in the principal stress space, indicating that the strength criterion should satisfy the Drucker's postulate, and could describe the physical properties of stable materials. The strength criterion can be expected to reflect the basic strength characteristics of hard rocks, such as the effects of intermediate principal stress, minimum principal stress, hydrostatic pressure, Lode angle, and tensile and compressive heterogeneity.

A generalized polyaxial strain energy (GPSE) strength criterion is proposed in this study, which is based on the basic rules and characteristics indicated by the results of hard rock test and Griffith's theory (Huang et al., 2008). In the octahedral space, the polyaxial strength criterion is expressed using octahedral normal stress σ_{oct}, shear stress τ_{oct}, Lode angle θ_σ, and uniaxial compressive strength f_c:

$$\frac{\tau_{oct}}{f_c} - F_{mp}\left(\frac{\sigma_{oct}}{f_c}\right)F_{octp}(\theta_\sigma) = 0 \quad (1)$$

where F_{mp} is the failure function of brittle rock on the meridian plane (Fig. 20); F_{octp} is the failure function of brittle rock on octahedral deviatoric plane, which is the smooth ridge model proposed by Yu et al. (2000). They can be expressed as follows:

$$F_{mp}\left(\frac{\sigma_{oct}}{f_c}\right) = \left[a^2\left(\frac{\sigma_{oct}}{f_c}\right)^2 + b\frac{\sigma_{oct}}{f_c} + c\right]^{0.5} \quad (2)$$

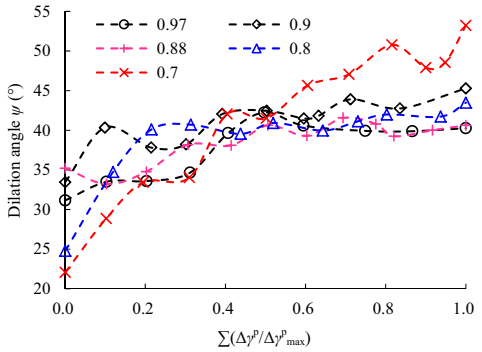

Fig. 18. Unloading dilation features of Jinping marble at different degrees of initial damage under the initial confining pressure of 20 MPa (Qiu et al., 2012).

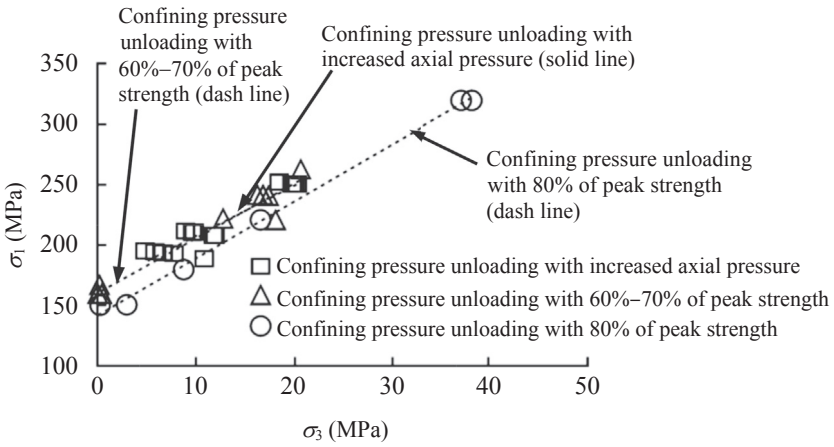

Fig. 19. Comparison of ultimate bearing strengths of Jinping marble under two unloading paths (Qiu et al., 2012).

$$F_{\mathrm{octp}}(\theta_\sigma) = \frac{2(1-\gamma^2)+(\gamma-2)\sqrt{4(\gamma^2-1)+(5-4\gamma)f_{\theta_\sigma}^2}}{4(1-\gamma^2)-(\gamma-2)^2 f_{\theta_\sigma}^2}\gamma f_{\theta_\sigma} \tag{3}$$

where γ is the ratio of triaxial tensile to compressive strength of rocks; and $f_{\theta_\sigma} = \sec(\pi/6-\theta_\sigma)$ $(-\pi/6 \le \theta_\sigma \le \pi/6)$; b and c are the material parameters.

Using the same test result, the precision of predictions by different strength criteria could be compared based on the fitting error. Colmenares and Zoback (2002) analyzed the standard deviation of average prediction errors of several strength criteria, e.g. Mohr-Coulomb, Hoek-Brown, modified Wiebols-Cook, modified Lade, Drucker-Prager, and Mogi criteria. The grid search method was used to determine the optimal fitting parameters of each criterion, and to produce the standard deviation of average fitting errors, as shown in Fig. 21. It shows that the GPSE criterion has a better fitting precision than the other criteria do.

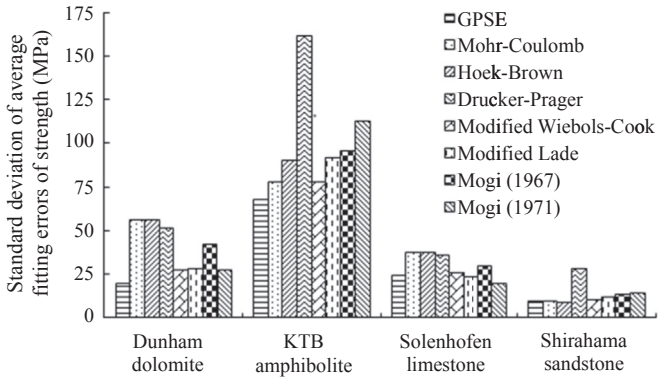

Fig. 21. Standard deviation of average fitting errors of strength by several strength criteria (Mogi, 1967, 1971).

8.3.3. Constitutive model

An elastoplastic strain-hardening and strain-softening constitutive model for hard rocks was established based on incremental elastoplastic theory (Zheng et al., 2002). It is here called the GPSEdshs constitutive model, and the GPSE criterion is adopted as the yield criterion (Huang, 2008). Using the non-associated flow rule, the plastic potential function is defined as follows:

$$g(\sigma_{ij},\kappa) = \tau_{\mathrm{oct}} + F_{\mathrm{octp}}(\theta_\sigma)K_\psi(\kappa)\sigma_{\mathrm{oct}} + t \tag{4}$$

where κ is the plastic internal variable; t is a constant; ψ is the dilatancy angle and K_ψ is a parameter describing dilatancy effect, i.e.

$$K_\psi = \frac{2\sqrt{2}\sin\psi}{3-\sin\psi} \tag{5}$$

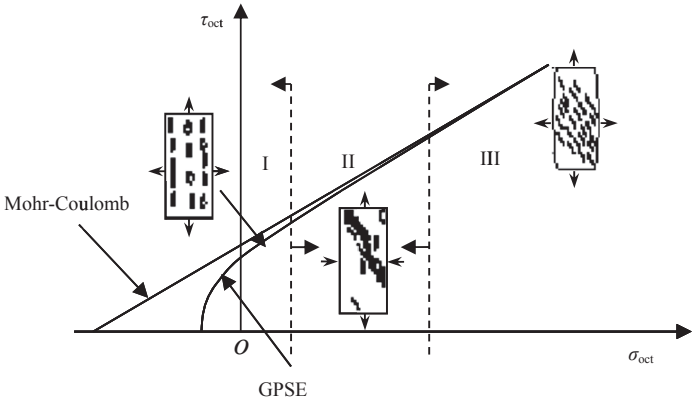

Fig. 20. Failure curves of GPSE criterion on meridian plane ($\theta_\sigma = 30°$). I, II and III denote the failure zones controlled by tensile micro-fracture, multiple mechanisms, and frictional slip, respectively.

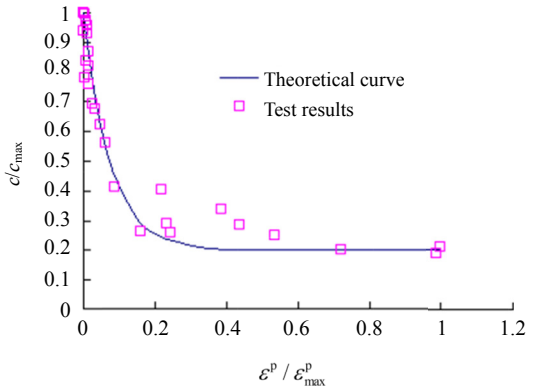

Fig. 22. Relationship of c–ε^p based on theoretical curve and test results of Jinping marble.

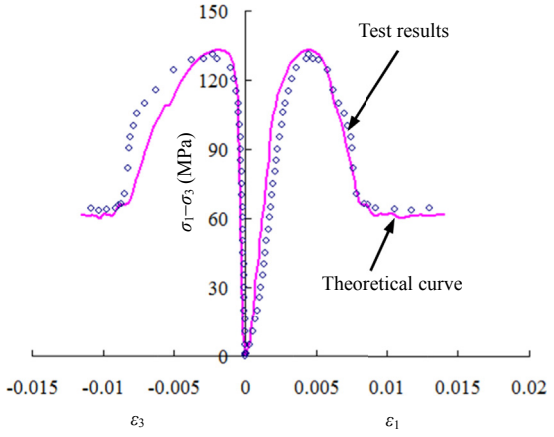

Fig. 23. Comparison between stress-strain curves of Jinping marble obtained by test and GPSEdshs model.

The hardening and softening laws are determined based on the cyclic loading and unloading test on hard rocks, as shown in Fig. 14. Huang (2008) found there is a negative exponential relationship between cohesion c and plastic volumetric strain $\widehat{\varepsilon}^p$, which can be expressed as follows:

$$c = c_{res} + (c_{pea} - c_{res})\left[\exp\left(-\varepsilon_v^p/\varepsilon_{v,c}^p\right)\right]^{n_c} \quad (6)$$

where c_{res} and c_{pea} are the residual and peak cohesions, respectively; ε_v^p is the plastic volume strain; $\varepsilon_{v,c}^p$ and n_c are the material parameters with respect to cohesion. It is here recommended that $n_c = 2$ and $\varepsilon_{v,c}^p = 0.15\%$. Fig. 22 compares the test results with the theoretical curve, which shows considerable consistency, suggesting that Eq. (6) is suitable to describe the evolution of cohesion c with plastic internal strain ε^p.

The variation of internal friction angle ϕ with plastic internal strain ε^p consists of an increasing stage and a decreasing stage. The functions of the increasing and decreasing stages can be expressed as a parabolic function and a negative exponential function, respectively:

$$\phi = \phi_{pea}\left(\frac{\varepsilon^p}{\varepsilon_{\phi 1}^p}\right)^{0.5} \quad \left(0 \le \varepsilon^p < \varepsilon_{\phi 1}^p\right) \quad (7)$$

$$\phi = \phi_{res} + \left(\phi_{pea} - \phi_{res}\right)\exp\left(-2\frac{\varepsilon^p - \varepsilon_{\phi 1}^p}{\varepsilon_{\phi 2}^p}\right) \quad \left(\varepsilon^p \ge \varepsilon_{\phi 1}^p\right) \quad (8)$$

where ϕ_{res} and ϕ_{pea} are the residual and peak internal friction angles, respectively; $\varepsilon_{\phi 1}^p$ and $\varepsilon_{\phi 2}^p$ are the material parameters of internal friction angle. On the basis of previous test results of deep marble, it is found that $\varepsilon_{\phi 1}^p = 0.15\%$ and $\varepsilon_{\phi 2}^p = 0.3\%$. Fig. 23 compares the test results with the theoretical curves under confining pressure of 30 MPa, where strong consistency is observed between them, suggesting that Eqs. (5) and (6) are suitable to describe the evolution of internal friction angle ϕ with plastic internal strain ε^p.

The evolution of the dilatancy parameter K_ψ with the plastic internal strain ε^p shows a rapidly increasing stage (reaching peak value with very small damage) and a slow decreasing stage. Because the increasing stage is short, it is assumed that the dilation angle of brittle rock starts from the peak value at initial damage. In other words, K_ψ is the highest at the beginning and then gradually decreases as the damage develops. The function is expressed in a negative exponential form:

$$K_\psi = K_{\psi,pea}\exp\left(-2\varepsilon^p\Big/\varepsilon_\psi^p\right) \quad (9)$$

where $K_{\psi,pea}$ is a peak dilatancy parameter, and ε_ψ^p is a material parameter that reflects the dilatancy effect.

Fig. 23 shows the agreement of stress-strain curves obtained using indoor test and prediction based on GPSEdshs constitutive model. It suggests that the proposed constitutive model can reflect strength characteristics, deformation characteristics, and deformation failure rule of deep hard rocks effectively.

Table 1
Mechanical parameters of rock mass of class III obtained by inversion method along the Jinping tunnel.

Stake range	Depth (m)	Rock type	Elastic modulus, E (GPa)	Poisson's ratio, ν	Initial cohesion, c_0 (MPa)	Residual cohesion, c_r (MPa)	Initial friction angle, ϕ_0 (°)	Final friction angle, ϕ_r (°)	Ultimate plastic shear strain corresponding to residual cohesion (%)	Ultimate plastic shear strain corresponding to final friction angle (%)
k15 + 250 in tunnel #3	1200	T_{2y}^4	15	0.23	8.9	3.3	27.7	44.6	0.4	0.9
k14 + 600–k14 + 950 in tunnel #2	1437–1585	T_{2y}^5	15	0.23	13.9	5.3	28.97	46	0.4	0.9
k14 + 300–k14 + 500 in tunnel #2	1637–1750	T_{2y}^5	15	0.23	13.2	5.3	28.97	46	0.4	0.9
k14 + 000–k14 + 200 in tunnel #4	1685–1720	T_{2y}^5	15	0.23	12	5.3	28.97	46	0.4	0.9
k13 + 250–k14 + 100 in tunnel #2	1730–1851	T_{2y}^5, T_{2y}^6	15	0.23	13.4	5.3	28.97	46	0.4	0.9
k13 + 750–k13 + 950 in tunnel #4	1760–1855	T_{2y}^5, T_{2y}^6	15	0.23	12.4	5.3	28.97	46	0.4	0.9
Baishan group marble		T_{2b}	18.9	0.23	15.6	7.4	25.8	39	0.45	0.9

Table 2
Mechanical parameters of rock mass of class II obtained by inversion method along the Jinping tunnel.

Stake range	Depth (m)	Rock type	Elastic modulus, E (GPa)	Poisson's ratio, ν	Initial cohesion, c_0 (MPa)	Residual cohesion, c_r (MPa)	Initial friction angle, ϕ_0 (°)	Final friction angle, ϕ_r (°)	Ultimate plastic shear strain corresponding to residual cohesion (%)	Ultimate plastic shear strain corresponding to final friction angle (%)
k13 + 085 in tunnel #2	1700	T^5_{2y}	25.3	0.22	18.9	8.5	23.4	40	0.3	0.6
k12 + 750–k13 + 150 and k14 + 150–k14 + 250 in tunnel #2	1680–1755	T^5_{2y}	25.3	0.22	21.3	8.5	23.4	40	0.3	0.6
k13 + 350–k13 + 600 in tunnel #4	1896–1936	T^5_{2y}	25.3	0.22	17.3	8.5	23.4	40	0.3	0.6

8.4. Identification of mechanical parameters of surrounding rocks

The Yantang formation mainly consists of marble T^4_{2y}, T^5_{2y}, and T^6_{2y}, and the Baishan formation consists of marble T_{2b}. These rock strata have different geological characteristics, such as color, thickness, and layered features, but they have similar mechanical properties. Because of the differences in thickness and tectonic influence, the developments of bedding plane and discontinuity of the two strata are different. In addition, the values of mechanical parameters of surrounding rocks vary at different positions in the same stratum. The macro-failure characteristics and modes of brittle marble under high stress condition have been well understood through observation and analysis of massive indoor tests and on-site failure events during the excavation, and they are used for the strategy of support design. While determining site-specific support parameters, the major concerns are the evaluation of degree and depth of failure. To fulfill the objective of a scientific design, it is important to investigate the mechanical parameters of rocks.

The mechanical parameters of rocks are usually obtained using direct estimation and inversion method based on on-site monitoring data. The excavation responses of hard rocks mainly involve surrounding rock damage, fracture and failure with small deformation. Considering the influences of various factors such as engineering geology and construction interference, the deformation-based parameter inversion method is not suitable for hard rock underground projects. In this paper, the intelligent inversion method for underground projects under high in situ stress is proposed based on the EDZ information (Jiang et al., 2008). This method adopts an intelligent algorithm based on the GA and back propagation artificial neural network (ANN). Through conducting tests, monitoring, and analysis with the basic mechanical parameters and initial stress fields, a number of schemes are proposed with the aid of orthogonal or uniform design method. Numerical simulation is performed by considering the excavation unloading effect. The calculated results are used to train the ANN, and a GA is used to search for the optimal neural network structure, thereby establishing the nonlinear mapping relationship between the basic variables and the EDZ range of rock mass. Then, the GA is used to conduct the global optimization, and to develop the optimal solutions for basic variables with minimum objective function.

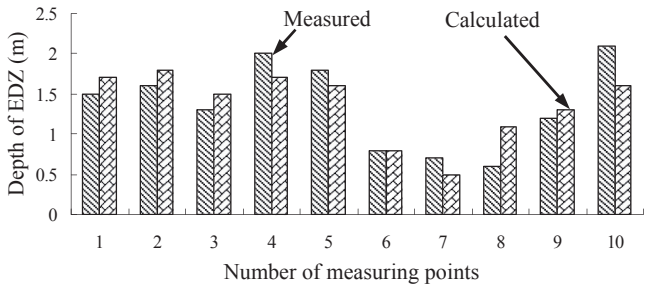

Fig. 24. Comparison between measured and calculated depths of EDZ at section k13 + 085 in headrace tunnel #2.

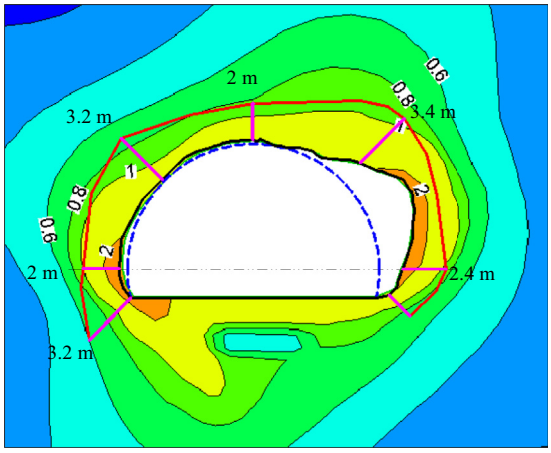

Fig. 25. Comparison between measured and calculated depths of EDZ at section k11 + 025 in headrace tunnel #2. Large-font bold numbers are the FAI values.

The mechanical parameters of different types of surrounding rocks at different sections of the headrace tunnels are determined using the inversion method based on the EDZ range obtained by acoustic wave test (Tables 1 and 2). The forward analytical calculation is performed using these parameters, and the results are compared to the on-site testing data. Figs. 24 and 25 show the comparisons of measured and calculated depths of EDZ at sections k13 + 085 and k11 + 025 in headrace tunnel #2, respectively. The calculated results are consistent with the test results, which indicate the rationality of determining parameters through acoustic wave test. In this way, it could serve as the basis of analysis for the stability of surrounding rocks in headrace tunnels.

8.5. Stability analysis of surrounding rocks

The analysis and evaluation of surrounding rocks stability are the basis for the design of support structure. After selecting accurate boundary conditions, suitable constitutive models, and reasonable mechanical parameters, the analytical results of surrounding rock stability can accurately reflect the stress-strain responses during excavation and support process. The evaluation results can be used to describe the range and degree of damage to surrounding rocks.

Generalized evaluation of the stability of the surrounding rocks not only reflects the stability of certain location or section, but also assesses the overall stability problems of the project. The former issue involves the whole project period before and after excavation, and the latter is the main concern during the planning stage. In this study, the minimum spacing of the headrace tunnels is

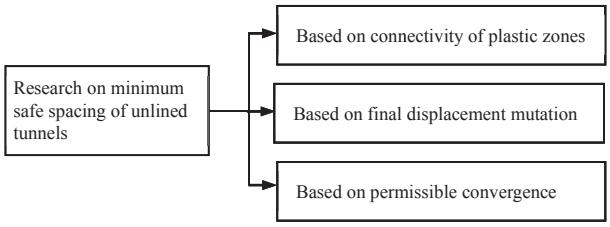

Fig. 26. Flowchart of research on minimum safe spacing between centerlines of headrace tunnels.

investigated. Then, based on the proposed stability evaluation index FAI, the stability analytical results of the surrounding rocks in the Jinping headrace tunnels are presented. Finally, the fracture inhibition method for the design of the rockbolt support parameters in the deep hard rock engineering is described, and its application is reported.

8.5.1. Minimum spacing of headrace tunnels

Before excavation of the headrace tunnels at the Jinping II hydropower station, two auxiliary tunnels were first excavated, and many technical difficulties were observed during the construction of two auxiliary tunnels. Several severe rockbursts occurred. The diameters of four headrace tunnels are designed to be 1.9 times greater than those of the auxiliary tunnels. For a single tunnel, the damage range is expected to exceed that of the auxiliary tunnel. If the spacing between four headrace tunnels is too small, the detectable interference will exist, which definitely increases the damage of the surrounding rocks, and even causes failure of all four tunnels. If the spacing is too large, the scale of powerhouse will also be expanded, affecting powerhouse stability and increasing the investment. In this way, determination of reasonable tunnel spacing is a key issue in both the feasibility research period and the design stage.

In this section, the overall technical flowchart for studying the minimum safe spacing of headrace tunnels is shown in Fig. 26. The search range is 30–70 m of central line distance. The initial deformation, ultimate deformation, and plasticity zone of surrounding rocks are determined for different spacings. Then, three standards including allowable deformation, connectivity of inter-tunnel plastic zones, and tendency of deformation variation at tunnel wall are used to determine the minimum safe spacing, which is capable of preventing the occurrence of overall failure of tunnel groups under the most unfavorable conditions.

Taking the connectivity of plastic zones in the surrounding rocks as the major concern, the minimum safe spacing of headrace tunnels is basically 30–35 m. When taking the mutation of deformation at the tunnel walls as the major concern, the minimum safe spacing is around 45 m. Taking the displacement exceeding the upper limit given by the Chinese specification as the controlling factor, the minimum safe spacing is 50 m. The above data suggest that the minimum safe spacing of the headrace tunnels should be 50 m. The design scheme finally selects the minimum safe spacing of 60 m to provide a certain safety margin.

8.5.2. Stability evaluation of surrounding rocks based on FAI

The stability analysis of surrounding rocks in deep hard rock projects involves two issues with respect to surrounding rocks, i.e. stress conditions and damage degree. The conventional index, i.e. strength-stress ratio, involves only one stress component; however, the actual surrounding rocks are subjected to 3D stress conditions. The plastic zone method is only able to show the range of damage to the surrounding rocks, whereas the damage degree within the damage range cannot be indicated. Hence, a new index is needed to describe the difference of the 3D surrounding rock stress and the damage degree.

Fig. 27. Failure state of surrounding rocks at section k9 + 810 in headrace tunnel #4.

Zhang et al. (2011) proposed a yield approach index (YAI) in 3D stress space through analyzing the spatial relationship between stress point and yield surface to evaluate the 3D stresses. They also proposed a FD index via investigating the evolution of plastic strain of rocks in loading failure process to describe the damage degree. The YAI and FD are integrated into FAI, and expressed as follows:

$$FAI = \begin{cases} \omega & (0 \le \omega < 1) \\ 1 + FD & (\omega = 1,\ FD \ge 0) \end{cases} \tag{10}$$

$$\omega = 1 - YAI = 1 - \frac{I_1 \sin\phi/3 + \left(\cos\theta_\sigma - \sin\theta_\sigma \sin\phi/\sqrt{3}\right)\sqrt{J_2} - c\cos\phi}{I_1 \sin\phi/3 - c\cos\phi} \tag{11}$$

$$FD = \overline{\gamma}_p \Big/ \overline{\gamma}_p^r \tag{12}$$

where I_1 is the first invariant of stress tensor, and $I_1 = \sigma_1 + \sigma_2 + \sigma_3$; J_2 is the second invariant of deviatoric stress tensor, and $J_2 = [(\sigma_1 - \sigma_2)^2 + (\sigma_2 - \sigma_3)^2 + (\sigma_3 - \sigma_1)^2]/6$; $\overline{\gamma}_p$ is the equivalent plastic shear strain of rocks, and $\overline{\gamma}_p = \sqrt{e_{ij}^p e_{ij}^p/2}$, in which e_{ij}^p is the plastic deviatoric strain; and $\overline{\gamma}_p^r$ is the ultimate plastic shear strain of rocks.

Fig. 12 shows the FAI distribution in the surrounding rocks at section k9 + 810 of headrace tunnel #4, and the actual surrounding rock damage situation is shown in Fig. 27. In Fig. 12, the area with $FAI > 2$ is the surrounding rock failure zone, $1 \le FAI < 2$ denotes the post-peak fracture softening zone, and $FAI < 1$ denotes the elastic zone. Comparing the EDZ obtained by the acoustic test with the area of $FAI = 1$ in Fig. 12, and also the failure of surrounding rocks at the foot of the arch in the south side in Fig. 27 with the area of

Table 3
Maximum damage depth of surrounding rocks at deep sections of headrace tunnels.

Rock type	Depth (m)	Rock class	Maximum damage depth (m)
Yantang group	1500	II	1.7
		III	3.1
	1900	II	3
		III	4.4
Baishan group	1900	II	1.9
		III	3.7
	2500	II	3.2
		III	4.8

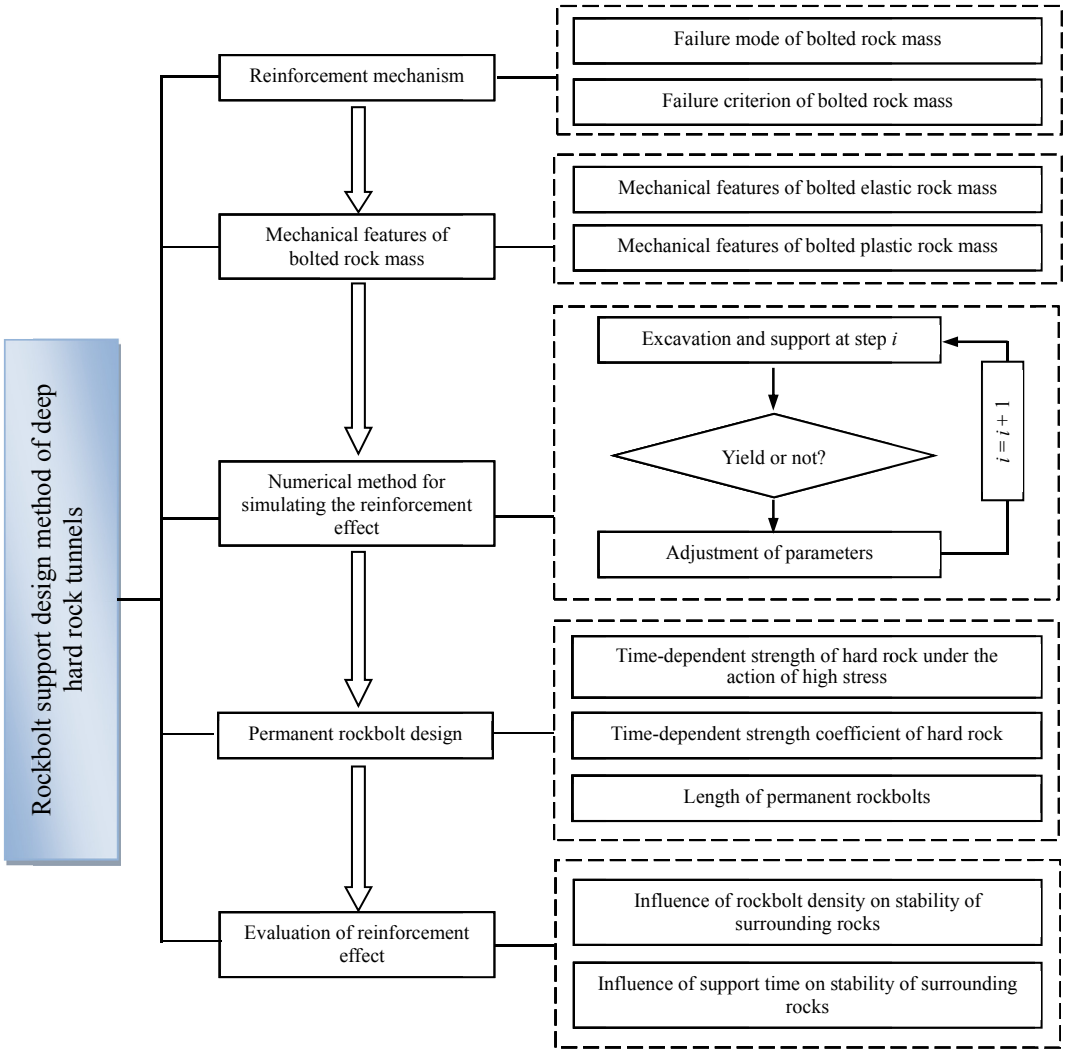

Fig. 28. Rockbolt support design method of deep hard rock tunnels (Wu et al., 2012).

$FAI = 2$ in Fig. 12, one can see that the FAI can accurately describe on-site surrounding rock damage and failure situation. The stability evaluation of surrounding rocks based on the FAI can provide a basic foundation for rockbolt support design in tunnels. The calculated maximum depth of surrounding rock damage and fracture at the tunnel section is shown in Table 3.

8.5.3. Rockbolt support design

The grouting rockbolts are used to improve the construction safety and long-term stability of surrounding rocks in the headrace tunnels of the Jinping II hydropower station. In deep hard rock tunnels, the function of rockbolts is to improve the stress conditions in the surrounding rocks, and to form a composite structure with surrounding rocks, thereby improving the mechanical properties of rocks. It is apparent that the mechanism of rockbolts in the underground projects is different from that in shallow projects.

A rockbolt support design method for deep hard rock tunnels is established, as shown in Fig. 28. It considers 3D dynamic processes of tunnel excavation and support. The failure criterion of bolted rocks is proposed based on the rock failure patterns. The computing methods for peak and post-peak strength parameters of yielded rock mass and elastic rock mass reinforced by bolts are recommended. Then, the mechanical parameters of surrounding rocks are dynamically adjusted in numerical simulations based on the sequences of excavation and support. Finally, combining with the stability evaluation index FAI, the influences of distribution density of rockbolts and support time of grouted rockbolts on surrounding rock stability are investigated (Feng et al., 2013b).

Determination of the mechanical parameters of bolted rock mass is the key to this rockbolt support design method. The mechanical parameters of the bolted elastic surrounding rocks can be computed by

$$c_0' = c_0 + \frac{\pi D^2 \sigma_s (1/2 + \phi_0/180)\sin(45^\circ + \phi_0/2)}{4\sqrt{3} s_a s_c} \tag{13}$$

$$\phi_0' = \arcsin\frac{B-1}{B+1},\quad B = \left(\frac{\sigma_c'}{\sigma_c}\right)^2 \left(\frac{c_0}{c_0'}\right)^2 \frac{1+\sin\phi_0}{1-\sin\phi_0} \tag{14}$$

where D is the rockbolt diameter; σ_s is the tensile strength of rockbolt; c_0 and ϕ_0 are the initial cohesion and internal friction angle of surrounding rocks, respectively; s_a and s_c are the spacing design parameters of the rockbolts along the axial and circumferential directions of the tunnel, respectively; σ'_c is the uniaxial

Table 4
FAI distribution of surrounding rocks bolted with different rockbolt spacings.

Rockbolt spacing, $s_a \times s_c$ (m × m)	Without rockbolt	Rockbolt with length of 3 m
1 × 1	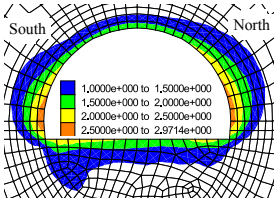	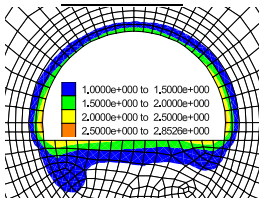
1 × 2	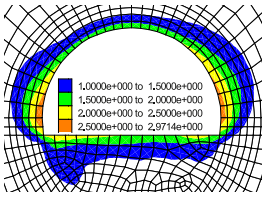	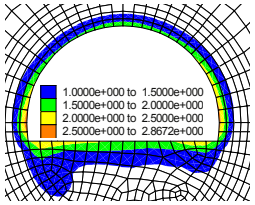
2 × 2	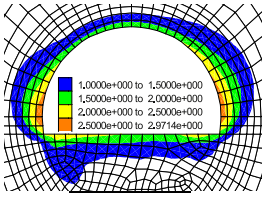	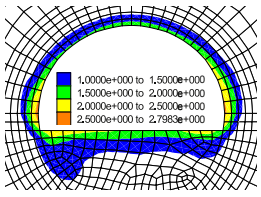

compressive strength of the rockbolts-surrounding rock composite structure; c'_0 and ϕ'_0 are the cohesion and internal friction angle before yielding of the composite structure, respectively.

After rock mass yields, the rock mass reinforcement effect can be expressed as follows:

$$\left.\begin{aligned} c'\left(\overline{\varepsilon^{\mathrm{p}}}\right) &= c\left(\overline{\varepsilon^{\mathrm{p}}}\right) + \Delta c'\left(\overline{\varepsilon^{\mathrm{p}}}\right) \\ \phi'\left(\overline{\varepsilon^{\mathrm{p}}}\right) &= \phi\left(\overline{\varepsilon^{\mathrm{p}}}\right) + \Delta\phi'\left(\overline{\varepsilon^{\mathrm{p}}}\right) \end{aligned}\right\} \tag{15}$$

where $c'(\overline{\varepsilon^{\mathrm{p}}})$ and $\phi'(\overline{\varepsilon^{\mathrm{p}}})$ are the cohesion and internal friction angle of the composite structure at certain equivalent plastic strain, respectively; $\Delta c'(\overline{\varepsilon^{\mathrm{p}}})$ and $\Delta\phi'(\overline{\varepsilon^{\mathrm{p}}})$ are the relative increments of cohesion and internal friction angle of the composite structure, respectively, which are both functions of equivalent plastic strain and can reflect the reinforcement effect. Table 4 shows the FAI distribution with different rockbolt spacings, which demonstrates the effectiveness of the proposed design method.

On-site surrounding rock fracture response and laboratory test results demonstrate that the surrounding rocks would experience time-dependent failure under long-term high stress conditions. The long-term strength is lower than the uniaxial and triaxial strengths. This would cause potential risk for tunnel safety during operation, and thus should be considered in rockbolt support design. It involves several key issues such as obtaining the long-term strength of hard rock and establishing the corresponding design method of rockbolt support. Martin (1997) reported that the long-term strength is only 80% of the uniaxial strength. By analyzing the triaxial test data of the Jinping marble, the relationship between the long-term strength coefficient α_1 and the confining pressure σ_3 is found to be

$$\alpha_1 = -0.0014\sigma_3 + 0.81 \tag{16}$$

Neglecting the first term of Eq. (16), we can see that the long-term strength of marble is 81% of the triaxial strength under triaxial conditions. Thus, the long-term safety factor of marble is written based on FAI as

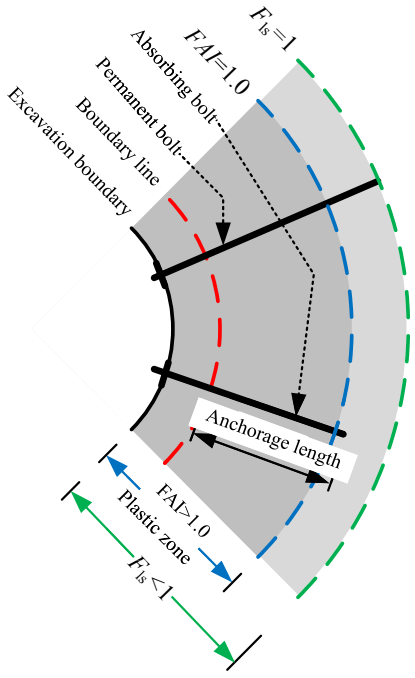

Fig. 29. Design of length of permanent rockbolts.

Table 5
Rockbolt parameters suggested in design of headrace tunnels.

Rock type	Depth (m)	Rock class	Theoretical length of rockbolts (m)	Suggested length of rockbolts (m)	Final designed length of rockbolt (m)	Initial designed length of rockbolt before construction (m)
Yantang group	1000	II	2.1	3	4.5	4.5
		III	3.5	4.5	4.5	4.5/6
	1500	II	2.4	3	4.5	4.5
		III	3.8	4.5	4.5	4.5/6
	1900	II	4.2	4.5	4.5/6	4.5/6
		III	5.6	6	4.5/6	6
Baishan group	1900	II	3.1	4.5	4.5/6	6
		III	4.9	6	6	6/8
	2500	II	4.4	4.5	6	6
		III	6	6	6	6/8

$$F_{ls} = \begin{cases} \dfrac{\alpha_l}{\sigma_1}\left(\dfrac{1+\sin\phi}{1-\sin\phi}\sigma_3 + \dfrac{2c\cos\phi}{1-\sin\phi}\right) & (\sigma_1 < \sigma_{ps}) \\ \alpha_l & (\sigma_1 = \sigma_{ps}) \end{cases} \quad (17)$$

The above equation indicates that in order to ensure the fracture inhibition effect of rockbolts on rock mass in the time-dependent EDZ, the rockbolts must be at least anchored in the area with $F_{1s} = 1$, as shown in Fig. 29.

The rockbolt support parameters are optimized for different sections of the headrace tunnels at the Jinping II hydropower station (Table 5). The rockbolt length is decreased from 8 m to 6 m for general sections and key sections with intense rockburst, respectively, and the rockbolt length is decreased from 10 m to 6/9 m for sections with extremely intense rockburst. These recommended parameters have been accepted and implemented in the design. Fig. 30 shows that, after the rockbolts are installed, the stability of surrounding rocks improves considerably, which increases the long-term stability of deep tunnel sections with high in situ stress.

8.6. Time-dependent damage effect and lining support design of hard rock tunnels

During the operation period, many unfavorable conditions can be encountered in the deep hard rock tunnels, such as long-term strength of hard rocks, high external water pressure, and coupling effect of external water and surrounding rocks. Therefore, reinforcing the headrace tunnel lining is necessary. However, these problems and associated controlling conditions are beyond the scope of current specifications and knowledge. It is urgent to establish a lining design method for deep tunnels.

Fig. 30. On-site support effect of rockbolts with parameters designed by proposed method in Fig. 28.

8.6.1. Necessity of lining support

In the initial support design of headrace tunnels, the rockbolts and shotcrete are used in the absence of secondary lining. However, the time-dependent damage problems in the surrounding rocks are frequently observed during excavation. Fig. 31 shows the acoustic test results of the hole #6 at the tunnel section k13 + 085 in the headrace tunnel #2 during different stages after excavation. As shown in Fig. 31, after excavation for 36 d, the EDZ in the surrounding rocks is 0.9 m in depth, which increases to 2.2 m after 186 d. In addition, the failures of intact or fairly intact rock mass, such as spalling and peeling, are observed about 200 m behind the tunnel face.

As shown in Fig. 32, after excavation for 4 months (i.e. 22 April 2009), the rockbolt stress at north wall of section k15 + 290 of headrace tunnel #2 shows a sudden drop at measuring points #1 (located in the rock mass 2 m from the tunnel wall) and #2 (located in the rock mass 4 m from the tunnel wall). The axial stress of rockbolt at measuring point #1 decreases to 0, and that at measuring point #2 drops from 169 MPa to 92 MPa. Similar situation is also observed in the stress gages at south wall. This indicates that the bond between rockbolt and grout might suffer partial or complete failure. The rockbolts in high stress state present a good support function to the surrounding rocks, which facilitates its stability. However, this also indicates a high risk of failure of the rockbolt system.

The time-dependent damage to the surrounding rocks might occur under long-term high stress conditions, and the rockbolt support system might fail. Only using shotcrete–rockbolt support system cannot ensure the long-term safety of the headrace tunnels, thus lining is considerably important in Jinping II hydropower station.

8.6.2. Analysis of lining support parameters

After excavation, the surrounding rocks close to the surface suffer severe fracture, resulting in greater permeability coefficient than the lining. As the stable seepage field forms, if the pressure-relief vents are not drilled in the lining, the water pressure at the back of lining will exceed the maximum sustainable external water pressure of lining, and thereby makes the lining fail. In order to reduce the water pressure at the back of lining, the high-pressure consolidation grouting is performed within 6–12 m depth of the surrounding rocks to decrease its permeability coefficient. However, the grouting circle cannot completely block the seepage channels of external water, so the permeability coefficient is still larger than that of lining. After formation of long-term seepage field, high external water pressure still can be expected.

After construction of grouting and lining, the long-term permeability is significantly different from that during the construction period. Under the constant total stress, the effective stress field eventually changes the responses of surrounding rocks such as fracture or deformation, which will affect the safety of the lining.

In the deep tunnel projects, the lining suffers extremely complicated stress conditions, such as the internal and external water pressures, rock mass fracture deformation, long-term creep deformation, and time-dependent fracture deformation. The pattern of interaction between lining and surrounding rocks has changed from simple loading-structure relationship to strong coupling effect, i.e. the lining bears the compressive stress imposed by the surrounding rocks, and it provides supporting force to surrounding rocks. As the confining pressure increases, the strength of surrounding rocks increases, while the deformation decreases and even stops, leading to a constant pressure on the lining. With appropriate support parameters, the lining and surrounding rocks can finally reach a stable condition. For this reason, the coupling

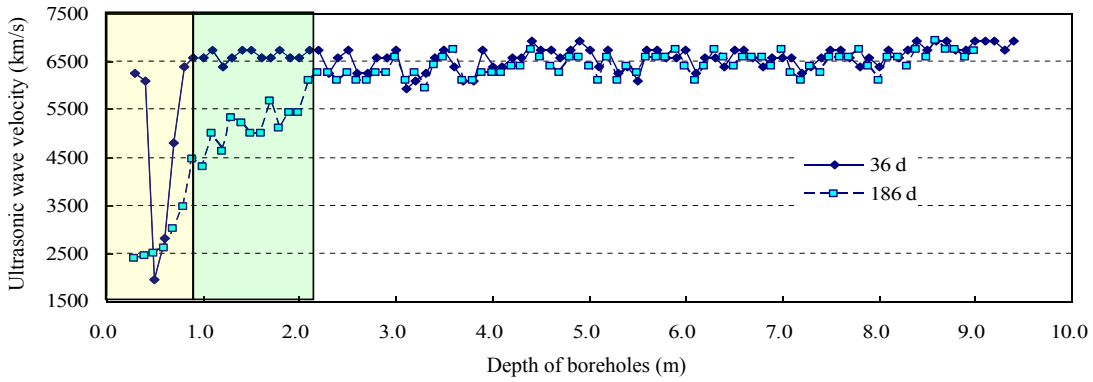

Fig. 31. Ultrasonic wave velocities along borehole #6 at section k13 + 085 in headrace tunnel #2.

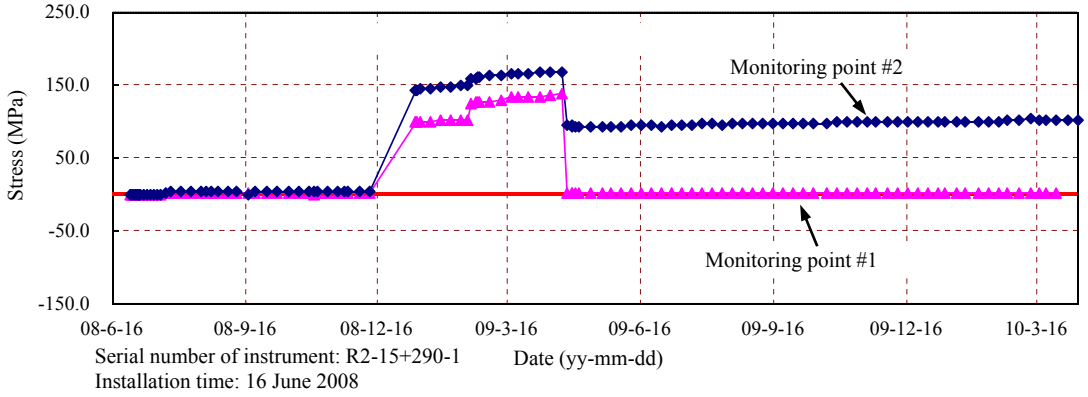

Fig. 32. Monitoring results of rockbolt stress at north side of section k15 + 290 in headrace tunnel #2.

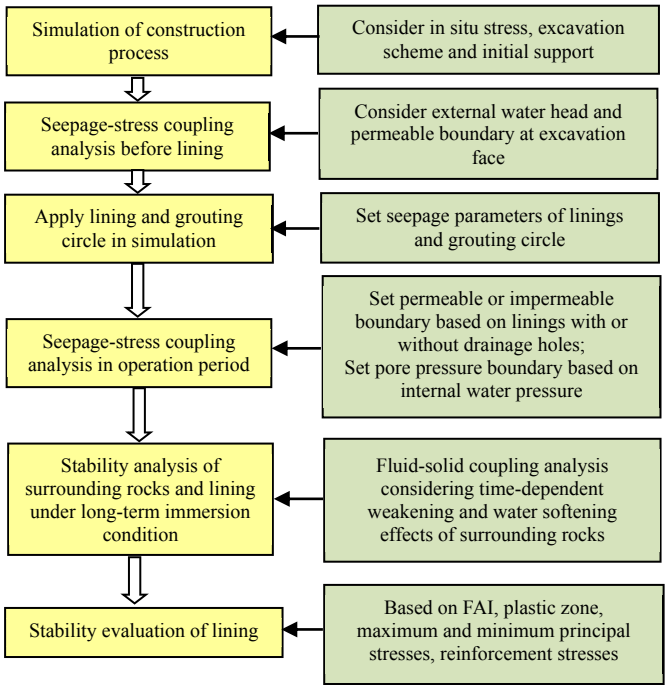

Fig. 33. Analysis of lining stability in deep hard rock tunnels in operation period.

effect between lining and surrounding rocks must be considered during the lining support design of deep tunnels.

In most commercial software and specifications, the lining is treated as a structural component. However, it is a composite structure of concrete and rebar. Moreover, the distribution of rebar is not uniform. Thus, it is herein proposed that solid elements are used to simulate the lining, i.e. solid elements for concrete and cable element for rebar. The fluid-solid coupling numerical simulation is used to analyze the safety of the lining during the operation stage of deep tunnels, as shown in Fig. 33. This method consists of six steps, i.e. simulation of construction process, seepage-stress coupling analysis before lining, lining construction and grouting circle setup, seepage-stress coupling analysis in operation period, safety analysis of lining of submerged surrounding rocks, and evaluation of lining stability.

For tunnel section at the depth of 2500 m, the relationship among the lining safety factor, lining thickness and maximum compressive stress is given (Table 6). The optimal lining thickness for this section is 0.8 m. Similarly, the lining thickness for deep tunnel sections at depths of 2000 m and 1900 m is 0.6 m. These

Table 6
Maximum pressures and safety factors of lining with different lining thicknesses at the depth of 2500 m.

Lining thickness (m)	Maximum pressure in lining (MPa)	Safety factor
0	–	–
0.6	14.2	0.9
0.8	9.8	1.3
1	7.8	1.6
1.2	5.9	2.1

parameters have been accepted by the designer. After 2 years' operation, the lining performance is satisfactory without large failure.

9. Conclusions

In this study, the dynamic design method of deep hard rock tunnels is proposed and applied to the deep headrace tunnels at the Jinping II hydropower station during the planning and construction periods. The major conclusions are drawn as follows:

(1) The dynamic design method of deep hard rock tunnels contains seven steps concerning the Jinping II project.
(2) According to the studies of the mechanical behaviors of excavation unloading of deep hard rocks, the triaxial cyclic loading and unloading testing methods in the axial and radial directions are established. The loading and unloading tests on Jinping marble are performed systematically at different stress levels and paths to reveal the deformation failure mechanisms and the coupling effects of various scenarios. Test results show that, as the damage degree increases, the elastic modulus and cohesion of marble decrease, and the internal friction angle increases. Based on this, new hard rock strength criterion and constitutive model are proposed.
(3) The identification method of in situ stresses along the deep long tunnels in the areas with strong tectonic movements is proposed, including analysis of tectonic movement history, current topography and formation of incised valleys, nonlinear inversion method of 3D in situ stress fields, and rationality validation of in situ stress field.
(4) The intelligent dynamic inversion method to determine the mechanical parameters of surrounding rocks in deep hard rock tunnels is proposed considering the evolution of cohesion and internal friction angle of rocks with unloading damage. The inversion analysis is performed based on the EDZ information obtained by the acoustic wave test. The mechanical parameters obtained by the inversion method can reasonably reflect the characteristics of the fracturing process of hard rocks.
(5) A new evaluation index FAI is proposed to describe the difference in FD of deep rocks at different positions and its evolution. It also can be used to analyze the fracture process of deep hard rocks and the mechanism of inhibition. The excavation and support optimization design method, i.e. the fracture-inhibition method, is proposed. Considering the long-term damage effect of deep hard rocks, the rockbolt support parameters of the deep headrace tunnels at the Jinping II hydropower station are recommended. The method of assessing lining safety in the deep hard rock tunnels during operation stage is established to optimize the thicknesses of the lining at different tunnel sections. The results of the study can provide references for the design of deep underground projects and for dealing with the key issues during the design and operation periods.

Conflict of interest

We wish to confirm that there are no known conflicts of interest associated with this publication and there has been no significant financial support for this work that could have influenced its outcome.

Acknowledgments

The authors gratefully acknowledge the financial support from the National Natural Science Foundation of China (Grant Nos. 50920105908, 41172282). The work in this paper is also supported by research fund from the Yalong River Hydropower Development Company, Ltd. We are also grateful for the support and assistance of the engineers at the HydroChina Huadong Engineering Corporation Limited.

References

Colmenares LB, Zoback MD. A statistical evaluation of intact rock failure criteria constrained by polyaxial test data for five different rocks. International Journal of Rock Mechanics and Mining Sciences 2002;39(6):695–729.
Feng XT, Chen B, Zhang C, Li SJ, Wu SY. Mechanism, warning and dynamic control of rockburst development processes. Beijing, China: Science Press; 2013a (in Chinese).
Feng XT, Zhang C, Li SJ, Qiu SL, Zhang CS. Dynamic design method for deep tunnels in hard rock. Beijing, China: Science Press; 2013b (in Chinese).
Huang S, Feng XT, Zhang C. A new generalized polyaxial strain energy strength criterion of brittle rock and polyaxial test validation. Chinese Journal of Rock Mechanics and Engineering 2008;27(1):124–34 (in Chinese).
Huang S. Study of mechanical model of brittle rock under high stress condition and its engineering application. PhD Thesis. Wuhan, China: Institute of Rock and Soil Mechanics, Chinese Academy of Sciences; 2008 (in Chinese).
Jiang Q, Feng XT, Chen G. Study of constitutive model of hard rock considering surrounding rock deterioration under high geostresses. Chinese Journal of Rock Mechanics and Engineering 2008;27(1):144–52 (in Chinese).
Martin CD. Seventeenth Canadian Geotechnical Colloquium: the effect of cohesion loss and stress path on brittle rock strength. Canadian Geotechnical Journal 1997;34(5):698–725.
Mogi K. Effect of the intermediate principal stress on rock failure. Journal of Geophysical Research 1967;72:5117–31.
Mogi K. Fracture and flow of rocks under high triaxial compression. Journal of Geophysical Research 1971;76:1225–69.
Qiu S, Feng XT, Zhang C, Yang J. Experimental research on mechanical properties of deep marble under different initial damage levels and unloading paths. Chinese Journal of Rock Mechanics and Engineering 2012;31(8):1686–97 (in Chinese).
Qiu S, Feng XT, Zhang C, Zhou H, Sun F. Experimental research on mechanical properties of deep-buried marble under different unloading rates of confining stress. Chinese Journal of Rock Mechanics and Engineering 2010;29(9):1807–17 (in Chinese).
Wu S, Shen M, Wang J. Jinping hydropower project: main technical issues on engineering geology and rock mechanics. Bulletin of Engineering Geology and the Environment 2010;69(3):325–32.
Wu W, Feng XT, Zhang C, Qiu S, Li Z. Reinforcing mechanism and simulating method for reinforcing effects of systemically grouted bolts in deep-buried hard rock tunnels. Chinese Journal of Rock Mechanics and Engineering 2012;31(Supp. 1):2711–21 (in Chinese).
Yu M, Zan Y, Fan W, Zhao J, Dong Z. Advances in strength theory of rock in 20th century – 100 years in memory of the Mohr-Coulomb strength theory. Chinese Journal of Rock Mechanics and Engineering 2000;19(5):545–50 (in Chinese).
Zhang C, Zhou H, Feng XT. An index for estimating the stability of brittle surrounding rock mass – FAI and its engineering application. Rock Mechanics and Rock Engineering 2011;44(4):401–14.
Zhang K, Zhou H, Pan PZ, Shen LF, Feng XT. Characteristic of strength of rocks under different unloading rates. Rock and Soil Mechanics 2010;31(7):2072–8 (in Chinese).
Zheng Y, Shen Z, Gong X. Geotechnical plastic mechanics principle. Beijing, China: China Building Industry Press; 2002 (in Chinese).

Xia-Ting Feng obtained his BSc degree in mining engineering from the Northeast University of Science and Technology in Shenyang, China, in 1986 and his PhD in rock mechanics from the Northeastern University, China, in 1992. Then he has been affiliated as Lecturer, Associate Professor (from 1993 to 1996) and Professor (from 1996 to 2001) at the same university, from September 1995 to March 1996 as a Visiting Researcher and from December 1996 to November 1997 as a ITIT Special Research Officer at National Institute for Resource and Environment, Tsukuba, Japan, and from May to November 1996 as a Senior Research Officer at Department of Mining Engineering, the University of Witwatersrand, South Africa. As a Professor of Hundred Talent Program of the Chinese Academy of Sciences, he joined Institute of Rock and Soil Mechanics, the Chinese Academy of Sciences in 1998, from 2001 to 2003 as Vice Director in Charge and from 2003 to 2005 as Director of this institute, from 2001 to 2007 as Director of Key Laboratory of Rock and Soil Mechanics, Chinese Academy of Sciences, from 2007 to present as Director of State Key Laboratory of Geomechanics and Geotechnical Engineering. He worked in Imperial College, UK, the University of Oklahoma, USA, Royal Institute of Technology, Sweden, and Lille University of Science and Technology, France as a Visiting Professor or Academic Visitor in short term. From 2011 to 2015 he is President of International Society for Rock Mechanics (ISRM), and from 2012 to present he is President of Chinese Society for Rock Mechanics and Engineering (CSRME).